6538–6550 *Nucleic Acids Research, 2019, Vol. 47, No. 12* *Published online 27 May 2019*
doi: 10.1093/nar/gkz409

Delicate structural coordination of the Severe Acute Respiratory Syndrome coronavirus Nsp13 upon ATP hydrolysis

Zhihui Jia[1,†], Liming Yan[1,†], Zhilin Ren[2], Lijie Wu[3], Jin Wang[4], Jing Guo[5], Litao Zheng[1], Zhenhua Ming[6], Lianqi Zhang[1], Zhiyong Lou[1] and Zihe Rao[1,2,3,*]

[1]Laboratory of Structural Biology, School of Medicine, Tsinghua University, Beijing 100084, China, [2]State Key Laboratory of Medicinal Chemical Biology, College of Life Science, Nankai University, Tianjin 300353, China, [3]Shanghai Institute for Advanced Immunochemical Studies and iHuman Institute, ShanghaiTech University, Shanghai 201210, China, [4]State Key Laboratory of Biotherapy, West China Hospital, Sichuan University, Chengdu 610041, China, [5]Protein Chemistry Facility, Center for Biomedical Analysis of Tsinghua University, Beijing 100084, China and [6]State Key Laboratory of Conservation and Utilization of Subtropical Agro-Bioresources, College of Life Science and Technology, Guangxi University, Nanning, China

Received February 05, 2019; Revised May 01, 2019; Editorial Decision May 02, 2019; Accepted May 25, 2019

ABSTRACT

To date, an effective therapeutic treatment that confers strong attenuation toward coronaviruses (CoVs) remains elusive. Of all the potential drug targets, the helicase of CoVs is considered to be one of the most important. Here, we first present the structure of the full-length Nsp13 helicase of SARS-CoV (SARS-Nsp13) and investigate the structural coordination of its five domains and how these contribute to its translocation and unwinding activity. A translocation model is proposed for the Upf1-like helicase members according to three different structural conditions in solution characterized through H/D exchange assay, including substrate state (SARS-Nsp13-dsDNA bound with AMPPNP), transition state (bound with ADP-AlF_4^-) and product state (bound with ADP). We observed that the β19–β20 loop on the 1A domain is involved in unwinding process directly. Furthermore, we have shown that the RNA dependent RNA polymerase (RdRp), SARS-Nsp12, can enhance the helicase activity of SARS-Nsp13 through interacting with it directly. The interacting regions were identified and can be considered common across CoVs, which provides new insights into the Replication and Transcription Complex (RTC) of CoVs.

INTRODUCTION

The emergence of Severe Acute Respiratory Syndrome coronavirus (SARS-CoV) in 2003 was the first opportunity to allow investigation of a coronavirus (CoV) that was a severe human pathogen. A decade later, a similar coronavirus termed Middle East Respiratory Syndrome Coronavirus (MERS-CoV) emerged, but alarmingly this virus has higher case-fatality rates than SARS-CoV. Thus, there is a refocussing of the world's attention onto CoVs. The fact that no therapeutic treatments are available for CoVs is a serious concern (1,2). It is therefore necessary to study the life cycle of CoVs to develop new ideas for effective vaccines or drugs.

SARS-CoV belonging to the genus Betacoronavirus in the family Coronaviridae has one of the largest known RNA genomes (∼29.7 kb) among RNA viruses. Two large polyproteins pp1a and pp1ab are encoded by this genome. After being proteolytically processed, 16 non-structural proteins (Nsps) are produced including primase (Nsp8), RNA-dependent RNA polymerase (Nsp12) and helicase (Nsp13). These three enzymes and other Nsps are components of a replication and transcription complex (RTC) which is essential for the life cycle of SARS-CoV (3,4).

Helicase SARS-CoV Nsp13 (SARS-Nsp13) plays a vital role in catalyzing the unwinding of duplex oligonucleotides into single strands in an NTP-dependent manner. Importantly, SARS-Nsp13 has been identified as an ideal target for the development of anti-viral drugs due to its sequence conservation and indispensability across all CoV species (5–7). SARS-Nsp13 has been characterized as belonging to superfamily 1 (SF1) of the six helicase superfamilies which are

*To whom correspondence should be addressed. Tel: +86 10 62771493; Fax: +86 10 62773145; Email: raozh@mail.tsinghua.edu.cn
†The authors wish it to be known that, in their opinion, the first two authors should be regarded as Joint First Authors.

classified on the basis of several conserved motifs and can unwind both RNA and DNA duplexes in the 5′ to 3′ direction (8). The associated NTPase activity can target all natural nucleotides and deoxynucleotides as substrates (9,10). Moreover, it has been shown that SARS-Nsp12 can enhance the helicase activity of SARS-Nsp13 by increasing the step size of nucleic acid (dsRNA or dsDNA) unwinding by 2-fold (11). However, how the SARS-Nsp12 increase its helicase activity and if the NTPase activity is also influenced remains unclear.

Structures of helicases from SF1 are available, amongst which the Upf1, eukaryotic RNA helicase essential for nonsense-mediated mRNA decay (NMD) signal pathway and Nsp10, the helicase of equine arteritis virus (EAV) share many structural features (12,13). SARS-CoV Nsp13 is also a Upf1-like helicase. However, until recently when the MERS-CoV Nsp13 was solved, no structural information for this coronavirus helicase was available despite biochemical characterization and the determination of kinetic parameters associated with its helicase or NTPase activity (14). The structure of MERS-CoV helicase in the absence of nucleotide and substrate was reported to have four domains, an N-terminal CH domain, two helicase core domains RecA1 and RecA2 and an inserted domain 1B. In addition, there is a 'stalk' region which connects the CH domain and 1B domain. However, how the five domains cooperate to contribute to the helicase function remains undefined.

Here, we first present the structure of the full-length SARS-CoV Nsp13 (SARS-Nsp13). The five domains including zinc-binding domain, stalk domain, 1B domain, 1A domain and 2A domain are shown to coordinate with each other to complete the final unwinding process. Helicases have been characterized as translocases as the unwinding activity can be the result of it translocating on single-stranded oligonucleotides (15). We demonstrate how the 1A and 2A domains coordinate with each other when SARS-Nsp13 translocates on ssDNA through observing the H/D exchanges conditions of three states of SARS-Nsp13 with different ligands bound including ATP analog (AMPPNP), ADP-AlF4$^-$ and ADP. Moreover, we show that SARS-Nsp13 can interact with SARS-Nsp12 with high affinity and identified the key interaction domain on SARS-Nsp13, which provides us with insight into the RTC of SARS-CoV.

MATERIALS AND METHODS

Protein expression and purification

The full-length helicase SARS-Nsp13 (1–601aa) was encoded by nucleotides (GenBank accession no. AY291315) of the SARS-CoV genome from strain Frankfurt 1 and was inserted into the modified pET-28a vector at NcoI/XhoI restriction sites with a hexa-histidine tag attached at its N-terminal end. BL21(DE3) cells were then transformed by introduction of this plasmid. After enlarging the reproduction volume of competent cells, the target gene was overexpressed. Cells were grown at 37°C and induced with 200 μM IPTG when the OD value reached ∼0.8. Thereafter, the induced cells were transferred to 18°C to grow for 12–16 h. Cells were harvested at 4500 rpm by centrifugation at 4°C. After ultrasonification and centrifugation at 14 000 rpm, the supernatant was run through a Ni-affinity column and the protein eluted with 200 mM imidazole. The eluate was then further purified by ion exchange column Hitrap S and size-exclusion chromatography (Superdex 200, GE Healthcare).

Crystallization, data collection and structure determination

The protein solution was collected and concentrated to 6.7 mg/ml and then incubated with 25 thymine single-stranded DNA(dT25) at a molar ratio of 1:1.2 and then incubated with 2 mM AMPPNP at 4°C for 3 h. The hanging-drop vapor-diffusion method was used to grow the Nsp13 crystals. The conditions for optimal crystal growth were 12% (w/v) polyethylene glycol 20 000, 2 M ammonium sulfate and 0.1 M MES monohydrate pH 6.5 at 16°C. The protein and this crystallization buffer were mixed in equal volumes.

All diffraction data sets were collected on beamline BL19U at Shanghai Synchrotron Radiation Facility (SSRF). Data was indexed, integrated and scaled with XDS (16). Single-wavelength anomalous data were collected at the zinc absorption edge and SHELXD was used to locate the six zinc atoms (17). The density map was improved with solvent flattening module of PHENIX program (18). The initial model was manually built in COOT (19) and further refined in PHENIX. The final 153 residues (443–596) were fitted using molecular replacement module in PHENIX with the equivalent residues of MERS-Nsp13. The structure was refined to 2.8 Å resolution.

Data collection and processing statistics are summarized in Table 1.

Surface plasmon resonance (SPR) assay

100 μl of 20 μg/ml SARS-Nsp12 in sodium acetate buffer pH 4.5 was prepared to be amino coupled onto channel 2 of a CM5 chip and fixed through addition of 100 μl ETA in water. A gradient of SARS-Nsp13 was set up from 0.39 μM to 3.12 μM for four cycles of binding data measurements. 5 mM NaOH buffer was used for regeneration of the chip. The contact time and dissociation time were each set to 60 s. The experimental data and fitting data were processed with GraphPad Prism.

Nucleic acid unwinding assay

As for the helicase activity, dsDNA (5′-AATGTCTGAC GTAAAGCCTCTAAAATGTCTG-3′-BHQ, CY3-5′-CA GACATTTTAGAGG-3′) was used where the excitation wavelength was set to 547 nm and emission wavelength was set to 562 nm to detect fluorescence of CY3. 200 nM Nsp13 (final concentration) was added to the reaction buffer (50 mM HEPES 7.5, 20 mM NaCl, 4 mM $MgCl_2$, 1 mM DTT, 0.1 mg/ml BSA) to incubate with dsDNA and 20 μM trap ssDNA for 5 min. Then 2 mM ATP (final concentration) was added to initiate the helicase activity and the fluorescence value was recorded by Perkin-Elmer Envision.

ATPase assay

The ATPase assay was performed using the two enzyme coupling method as follows. The two enzymes, pyruvate kinase and L-lactate dehydrogenase (from Sigma) were added

Table 1. Data collection and refinement statistics

Parameters (data collection statistics)	SARS-Nsp13
Data collection statistics	
Cell parameters	
a (Å)	192.0
b (Å)	189.2
c (Å)	57.3
α, β, γ (°)	90.0, 102.9, 90.0
Space group	*C*2
Wavelength used (Å)	0.9798
Resolution (Å)	50.0–2.69 (2.72–2.69)[c]
No. of all reflections	222 454 (9905)
No. of unique reflections	21 016 (1065)
Completeness (%)	100.0 (100.0)
Average I/σ(I)	10.6 (2.33)
R_{merge}[a] (%)	10.4 (69.9)
Refinement statistics	
No. of reflections used ($\sigma(F) > 0$)	48 632
R_{work}[b] (%)	23.75
R_{free}[b] (%)	29.25
r.m.s.d. bond distance (Å)	0.014
r.m.s.d. bond angle (°)	1.811
Average *B*-value (Å^2)	61.49
No. of protein atoms	9,335
No. of ligand atoms	0
No. of solvent atoms	149
Ramachandran plot	
res. in favored regions (%)	79.52
res. in allowed regions (%)	15.51
res. in outlier regions (%)	4.97

[a] $R_{merge} = \Sigma_h \Sigma_I |I_{ih} - I_h| / \Sigma_h \Sigma_I I_h$ where I_h is the mean of observations I_{ih} of reflection *h*.
[b] $R_{work} = \Sigma(||F_p(obs)| - |F_p(calc)||)/\Sigma|F_p(obs)|$. R_{free} is an *R* factor for a pre-selected subset (5%) of reflections that was excluded in the refinement.
[c] Numbers in parentheses are corresponding values for the highest resolution shell.

to the 200 μl reaction buffer system with final concentration as 100 units/ml and 200 units/ml respectively. Phosphoenolpyruvate (PEP, from SIGMA) and NADH were also added as co-factors for enzyme coupling. 20 nM Nsp13 was incubated with a ssDNA in a buffer containing 50 mM MOPS pH 7.0, 10 mM $MgCl_2$ and 50 mM NaCl for 5 min. Varying concentrations of ATP were then added to initiate the reaction and the $OD_{340\,nm}$ value of NADH was measured using the Perkin-Elmer Envision. The K_m value was calculated using GraphPad Prism.

Hydrogen/deuterium exchange mass spectrometry (H/DX MS)

H/DX MS is an established method for protein–protein and protein-DNA interaction detection on peptide level (20). The exchange of amide backbone hydrogens for deuterons is monitored by mass spectrometry, and can be localized to specific peptides within the primary structure, upon proteolytic digestion. It can report on interaction related regions with backbone amide groups involved in interactions or sequestration of regions of a protein in a solvent-inaccessible hydrophobic core, as deuteration will require both exposure of the region to solvent and fluctuations in hydrogen bonding (21).

For the HD/X experiment, 5 μl of 0.7 μg/μl SARS-Nsp13 alone or in the presence of ligand was prepared. The pH of the buffer was 7.0, which contained 20 mM HEPES, 150 mM NaCl and 4 mM $MgCl_2$. To initiate deuterium labeling, 5 μl of each 2 μg/μl protein solution was diluted with 45 μl of labeling buffer (contents, 99% D_2O, pH 6.6) at 25 °C for 10 min, and 50 μl of ice-cold quench buffer (1% (v/v) formic acid in water solution, 100% H_2O) was added to quench the labeling. The reaction tube was then put on ice. 10 μl of 1 μM pepsin solution was added for digestion. After 5 min, the sample was centrifugated and placed into the auto-sampler of the Ultimate 3000 UPLC system (Thermo, CA, USA) for injection. 50 μl of sample was then loaded onto and separated by a ACQUITY UPLC 1.7 μm BEH C18 1.0 μm × 50 mm column (Waters). A 1–50% gradient of acetonitrile over 37 min at a flow rate of 100 μl/min was used to separate peptides. Both chromatographic mobile phases contained 0.1% (v/v) formic acid. Mass spectrometry analysis was performed on Q Exactive Orbitrap mass spectrometer (Thermo, CA). The hydrogen/deuterium exchange difference of each peptide between protein alone and protein with ligand was manually checked.

Electrophoretic mobility shift assay (EMSA)

To screen for an optimal substrate for Nsp13, we tested >20 nucleic acids, most of which originated from the sequence of the SARS genome. We conducted an electrophoretic mobility shift assay (EMSA) to see which nucleic acid had the strongest binding affinity for Nsp13. Finally, we identified one which originated from the first 38 nucleotides of Nsp7 of the SARS genome, named 7F (CATGCCATGGCCTC TAAAATGTCTGACGTAAAGTGCACATCTGT). The dsDNA we used in the helicase activity assay was also derived from 7F.

EMSA assay was performed to detect both the nucleic acid binding ability and unwinding activity. The buffer used for binding to incubate SARS-Nsp13 with nucleic acids contained 20 mM HEPES 7.0, 50 mM NaCl and 5 mM $MgCl_2$ while the buffer used for unwinding contained 20 mM HEPES 7.0, 50 mM NaCl, 5 mM $MgCl_2$, 0.1 mM DTT and 0.1 mg/ml BSA. After 30 min of incubation, 10× loading buffer consisting of 50% glycerol and 200 mM HEPES was added to each sample to prepare for the electrophoretic mobility (110 V), where the running buffer consisted of 25 mM Tris and 192 mM glycine (pH 8.2).

Docking the dsDNA on SARS-Nsp13 structure

NPDock server (22) docking program was used to predict the interactions between ATP–nsp13 complex and DNA. The double helix DNA fragments were constructed with the Nucleic Acid Builder (23) and used as the initial structures for the docking. NPDock performed global macromolecular docking with the default parameters and generated the 20 000 models. RMSD cut-off was set to 5 Å for clustering of the best-scored models. After refinement of protein–DNA contacts in the models, the best scoring models from the three largest clusters were selected for further analysis. And the score for dsDNA–Nsp13 complex model is –9.59,

which demonstrated that the model was confidential. Finally, the best pose with the highest probability was used to demonstrate the interaction between SARS-Nsp13 and dsDNA in PyMOL.

RESULTS

Overall structural description of SARS-Nsp13

Full-length SARS-Nsp13 (residues 1–601) was expressed in *Escherichia coli* with a hexa-histidine tag at the N-terminus. We confirmed that the SARS-Nsp13 expressed in *E. coli* can function normally with helicase and ATPase activity through nucleic acid unwinding assay and ATP hydrolysis assay (Figure 1C and D).

Similar to MERS-Nsp13, the overall structure of Nsp13 assumes a triangular pyramid shape consisting of five domains. Three domains including the two 'RecA-like' domains named 1A and 2A and the 1B domain are arranged to form the triangular base, leaving the remaining two domains including the N-terminal Zinc binding domain (ZBD) and the stalk domain directed towards the apex of the pyramid. The ZBD and 1B domains are connected through the stalk domain (Figure 1A).

There are two SARS-Nsp13 molecules in the asymmetric unit with the ZBD domain providing the interaction interface (Figure 1B). However, SARS-Nsp13 retains a monomer alone or with dsDNA (Supplementary Figure S1). Besides, the ZBD domains of two MERS-Nsp13 molecules do not contact each other at all (Figure 1B), indicating that the arrangement of the two SARS-Nsp13 molecules can be attributed to crystal packing.

The NTP hydrolysis active site

It has been shown that SARS-Nsp13 is an NTP-dependent SF1 helicase member. To better understand the NTPase active site, we identified six key residues involved in NTP hydrolysis through superimposition of SARS-Nsp13 with Yeast-Upf1-ADP-AlF_4^- (2XZL) (24), also belonging to SF1 family. The six residues, K288, S289, D374, E375, Q404 and R567, are highlighted in green color and cluster together in the cleft at the base between the 1A and 2A domains (Figure 2A).

Five of these residues, the exception being S289, are also conserved in MERS-Nsp13 and involved in nucleotide hydrolysis in the absence of a functional assay confirmation (14) (Supplementary Figure S2). Here, we tested the helicase activity on six single mutants. The results (Figure 2D–G) showed that the six mutants display highly unwinding deficiency. And the ATPase activity of the six mutants also decreased a lot as expected, amongst which S289A possessed the highest yet still much lower ATPase activity than that of wild type SARS-Nsp13 (WT-Nsp13) (Figure 2B). Initial ATP hydrolysis velocities of the six mutants are almost the same and lower than 50% of that of WT-Nsp13 (Figure 2C). The helicase activity of all six mutants are consistent with their ATPase activity indicating that the unwinding activity of SARS-Nsp13 is ATP hydrolysis dependent.

For MERS-Nsp13, Y442 has been proposed to stabilize the adenosine base of nucleotides (14). In SARS-Nsp13, it is replaced by arginine. So, here we made the R442A mutant and demonstrated that it has almost the same or even higher unwinding ability (Supplementary Figure S3). Thus, R442 does not participate directly in ATP hydrolysis.

Regions critical for double-stranded DNA (dsDNA) binding

To date, no helicase structure with a nucleic acid substrate for CoVs has been solved. In order to get detailed structural information about the nucleic acid binding regions, we docked a dsDNA on SARS-Nsp13 based on EAV-Nsp10-RNA structure (4N0O) (13) and Yeast-Upf1- RNA structure (2XZL) (24) (Figure 3A). It is evident that the radius of the channel formed by the 1B, 1A and 2A domains is not wide enough for dsDNA to pass through.

According to the artificial complex, residues 176–186 (1B domain), 209–214 (1B domain), 330–350 (1A domain) and 516–541 (2A domain) are the most probable nucleic acid binding regions (Figure 3A). We incubated SARS-Nsp13 with a 3-fold molar excess of dsDNA screened out from SARS-CoVs genome for H/D exchange assay. Four peptides that emerged from analyzing the results of H/D exchange assay all matched with the above four regions and demonstrated less H/D exchanges, indicating that they may possess dsDNA interacting amino acids (Figures 3B–E).

To further testify whether these regions affect the nucleic acid binding affinity, we constructed six double mutants including N179A/R212A, R337A/R339A, R507A/K508A, K524A/Q531A, K345A/K347A and S539A/Y541A and detected their binding activity for dsDNA using EMSA (Figure 4A and B). All the mutants exhibited binding deficiency except for mutant R507/K508 which showed almost the same binding affinity as WT SARS-Nsp13 (WT-13) (Figure 4C). We supposed that it is because of the special location of the two residues, R507 and K508. They are both situated on the surface of 2A domain and exposed to solution. When the two hydrophilic residues were mutated to alanines, the two hydrophobic alanines can cause the instability of the whole structure of SARS-Nsp13. The instability can be demonstrated through the DSF experiment (Supplementary Figure S5).

Furthermore, the helicase activity of all the six mutants suffered different degrees of deficiency, among which the mutant K345A/K347A exhibited the lowest activity with the two residues K345 and K347 belonging to the β19–β20 loop on domain 1A.

To discriminate whether the ten residues affected the helicase activity indirectly through involvement in the binding process or directly through involvement in the unwinding process, we incubated the SARS-Nsp13 with dsDNA and ssDNA separately for further H/D exchange assay. Intriguingly, amongst the four nucleic acid binding related peptides, only peptides 331–357 forming the β19–β20 loop where residues R337, R339, K345 and K347 are situated displayed no pattern shift when incubated with ssDNA. It is obvious that the β19–β20 loop on 1A domain plays a critical role during the unwinding process in a yet unknown way rather than binding and it does not necessarily participate in binding ssDNA when SARS-Nsp13 translocates on it (Supplementary Figure S4).

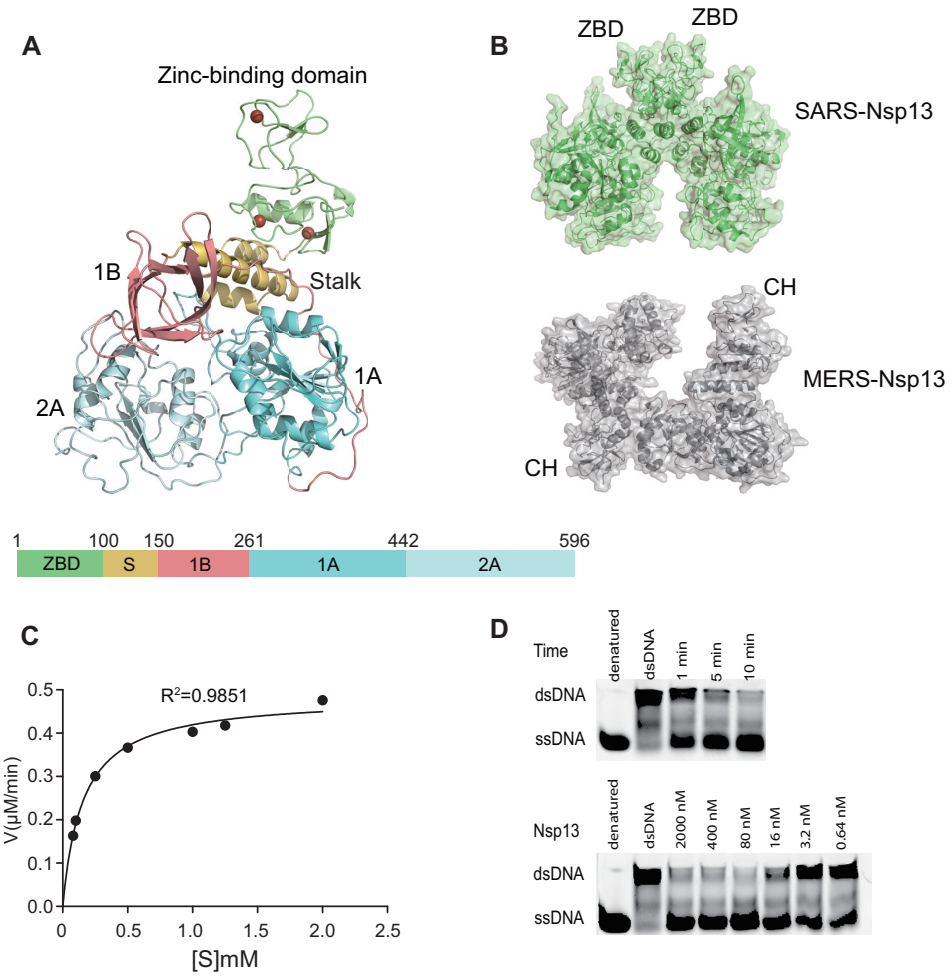

Figure 1. Overall structure of SARS-Nsp13. (**A**) Ribbon structure of SARS-Nsp13 is composed of ZBD (lime), stalk (yelloworange), 1B (salmon), 1A (aquamarine) and 2A (palecyan) domains. Three zinc atoms are shown as dark red spheres and schematic diagram of the domain organization of SARS-Nsp13. (**B**) Up, the crystal packing arrangement of two SARS-Nsp13 molecules. Down, the crystal packing arrangement of two MERS-Nsp13 molecules (5WWP). (**C**) The ATPase activity of SARS-Nsp13. The final concentration of SARS-Nsp13 was 25 nM. The gradient concentration of substrate ATP were 0.08, 0.1, 0.25, 0.5, 1.0, 1.25, 2.0 mM. The calculated V_0 corresponding to each ATP concentration was plotted against the ATP concentration fitting the Michaelis-Menten function. The final V_{max} is 0.4845 ± 0.01311 μM/min. K_m = 0.1552 ± 0.01693 mM. (**D**) The unwinding activity of SARS-Nsp13. Up, 20 nM SARS-Nsp13 was incubated with dsDNA for 1, 5 and 10 min. Down, SARS-Nsp13 of different concentrations were incubated with dsDNA for 1 min. The dsDNA (5′-CAGACATTTTAGAGG-3′-CY3, 5′-AATGTCTGACGTAAAGCCTCTAAAATGTCT-3′) used in the assay is labelled with CY3.

How can the 1A and 2A domains function on ssDNA along with ATP hydrolysis?

The nucleic acid binding channel and the nucleotide binding pocket have been verified through structural alignments and biochemical assays. To further understand how the 1B, 1A and 2A domains are involved in nucleic acid binding along with ATP hydrolysis, we artificially created four conditions where each signified a single structural state in a ATP hydrolysis cycle, Nsp13-dsDNA and Nsp13-dsDNA incubated with various ligands including ATP (AMPPNP), ADP-AlF_4^- and ADP. We performed the H/D exchange assay to check the shift patterns of five samples (plus ligand-free SARS-Nsp13). The relative shift D values of all the peptides with changed patterns are displayed on Supplementary Table S1.

The four conditions of SARS-Nsp13 with substrates are illustrated with different colors where red regions represented less H/D exchange (tightening) and blue regions represented more H/D exchange (loosening) compared to the previous condition in the ATP hydrolysis cycle. From this analysis, we can thus visualize the tightening or loosening state of specific regions in comparison to its previous state, gaining insights into the dynamic changes that are occurring (Figure 5).

We set the SARS-Nsp13-dsDNA as the initial state in the cycle with the whole structure in grey color. (Figure 5A). When ATP analog enters the active pocket, the 1A and 2A domains are pulled together. This is based on the fact that there is a reduced number of H/D exchanges in the region 427–437 (Supplementary Table S1). The region 427–437 (demonstrated in red in Supplementary Figure S6) is located in between the 1A and 2A domains. When we added the AMPPNP molecules in the incubation system, there were less H/D exchanges in this area, which indicated

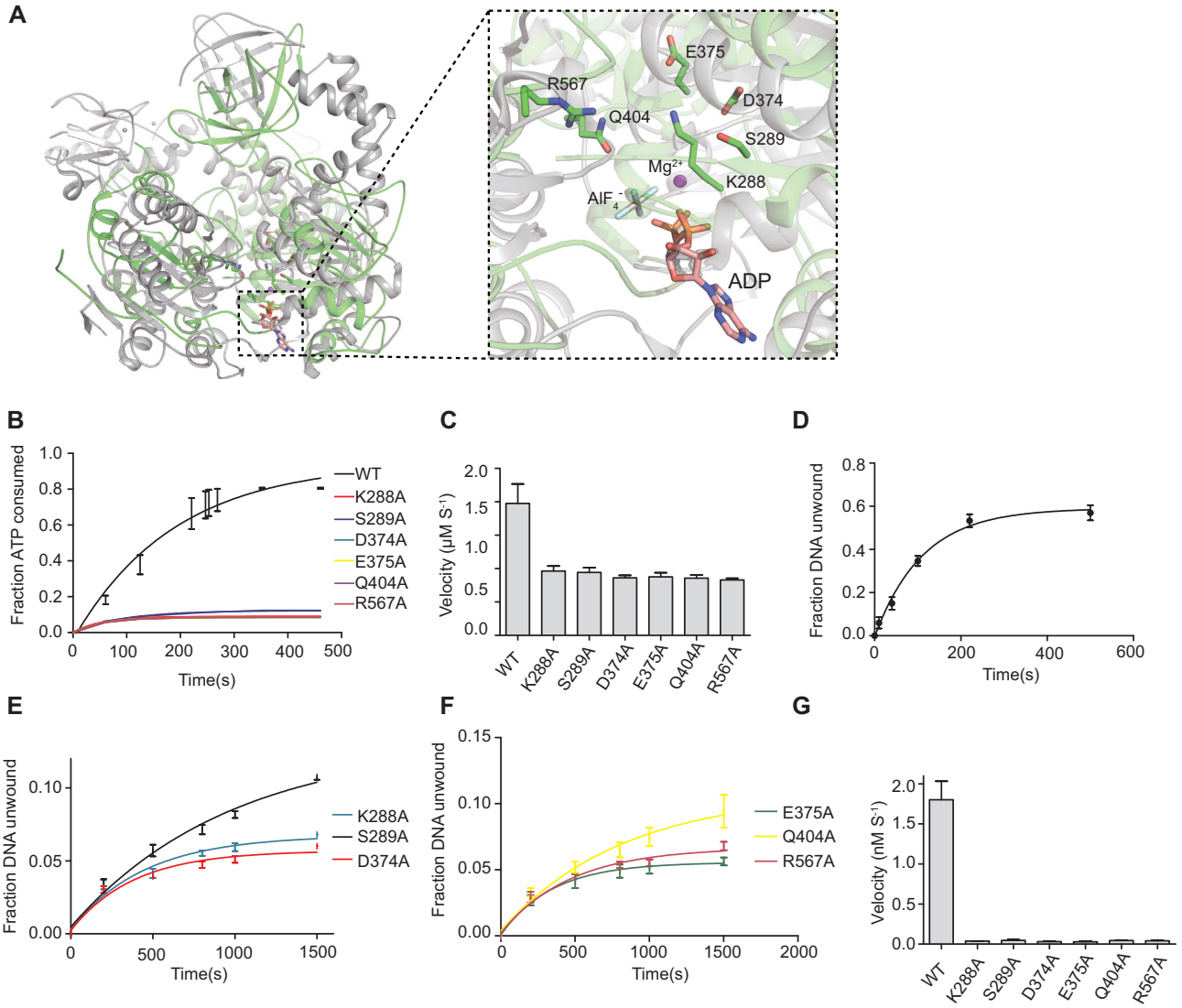

Figure 2. The active pocket composed of ATPase related residues. (**A**) Left, superposition between Yeast-Upf1-ADP-AlF_4^- (2XZL) (24) in grey and SARS-Nsp13 in green. Right, The stick model of all the ATPase related residues. The ADP-AlF_4^- is from the Upf1-ADP-AlF_4^- complex structure not the SARS-Nsp13 structure. AlF_4^- is presented in cyan while the ADP molecule in salmon. All the residues are presented in color by element with S atoms in orange, O atoms in red, N atoms in blue and H atoms in tints. (**B**) ATPase activity of all the ATP hydrolysis related mutants. The initial ATP concentration is 150 μM and the protein concentration is 25 nM. The changes of percentage of hydrolyzed ATP over time is demonstrated. The fitting function is one-phase association in the GraphPad Prism program. (**C**) Initial ATP hydrolysis velocities of WT-Nsp13 and six mutants under 150 μM ATP concentration are 0.3952 ± 0.05841 μM/s (WT-Nsp13), 0.1926 ± 0.01509 μM/s (K288A), 0.1884±0.01409 μM/s (S289A), 0.1725 ± 0.00748 μM/s (D374A), 0.1753 ± 0.0072 μM/s (E375A), 0.1716 ± 0.00947 μM/s (Q404A) and 0.1661 ± 0.005 μM/s (R567A) respectively. (**D**) The time-course changing of dsDNA unwound fraction for the WT-Nsp13. The initial dsDNA concentration is 250 nM and the protein concentration is 20 nM. The fitting function is one-phase association in the GraphPad Prism program. (**E**) The time-course changing of dsDNA unwound fraction for the three mutants including K288A, S289A, D374A. The initial dsDNA concentration is 250 nM and the protein concentration is 20 nM. The fitting function is one-phase association in the GraphPad Prism program. (**F**) The time-course changing of dsDNA unwound fraction for the three mutants including E375A, Q404A, R567A. The initial dsDNA concentration is 250 nM and the protein concentration is 20 nM. The fitting function is one-phase association in the Graphpad Prism program. (**G**) Initial unwinding velocities of WT-Nsp13 and six mutants under the dsDNA substrate concentration of 250 nM are 1.801 ± 0.2308 nM/s (WT-Nsp13), 0.037 ± 0.001212 nM/s (K288A), 0.04637 ± 0.008041 nM/s (S289A), 0.03097 ± 0.0049 nM/s (D374A), 0.02903 ± 0.007 nM/s (E375A), 0.04497 ± 0.00208 nM/s (Q404A) and 0.0407 ± 0.006129 nM/s (R567A) respectively.

that the surrounding structure around the region 427–437 became more tightened and less exposed to solvent. As a result, we inferred that the 1A domain and 2A domain might be pulled together when the AMPPNP molecule entered the active pocket. The ATP-bound substrate condition represented the finished changed state, which means the conformation change caused by ATP binding has already completed and is ready for the next step. The nucleic acid binding related peptides 511–542 and 496–511 showed less H/D exchanges indicating that more residues are involved in nucleic acid binding within these two regions. In contrast to the 2A domain, the 1A domain adopts a more relaxed structure with the two peptides placed within the nucleic acid binding channel, 318–330 and 358–369 having more H/D

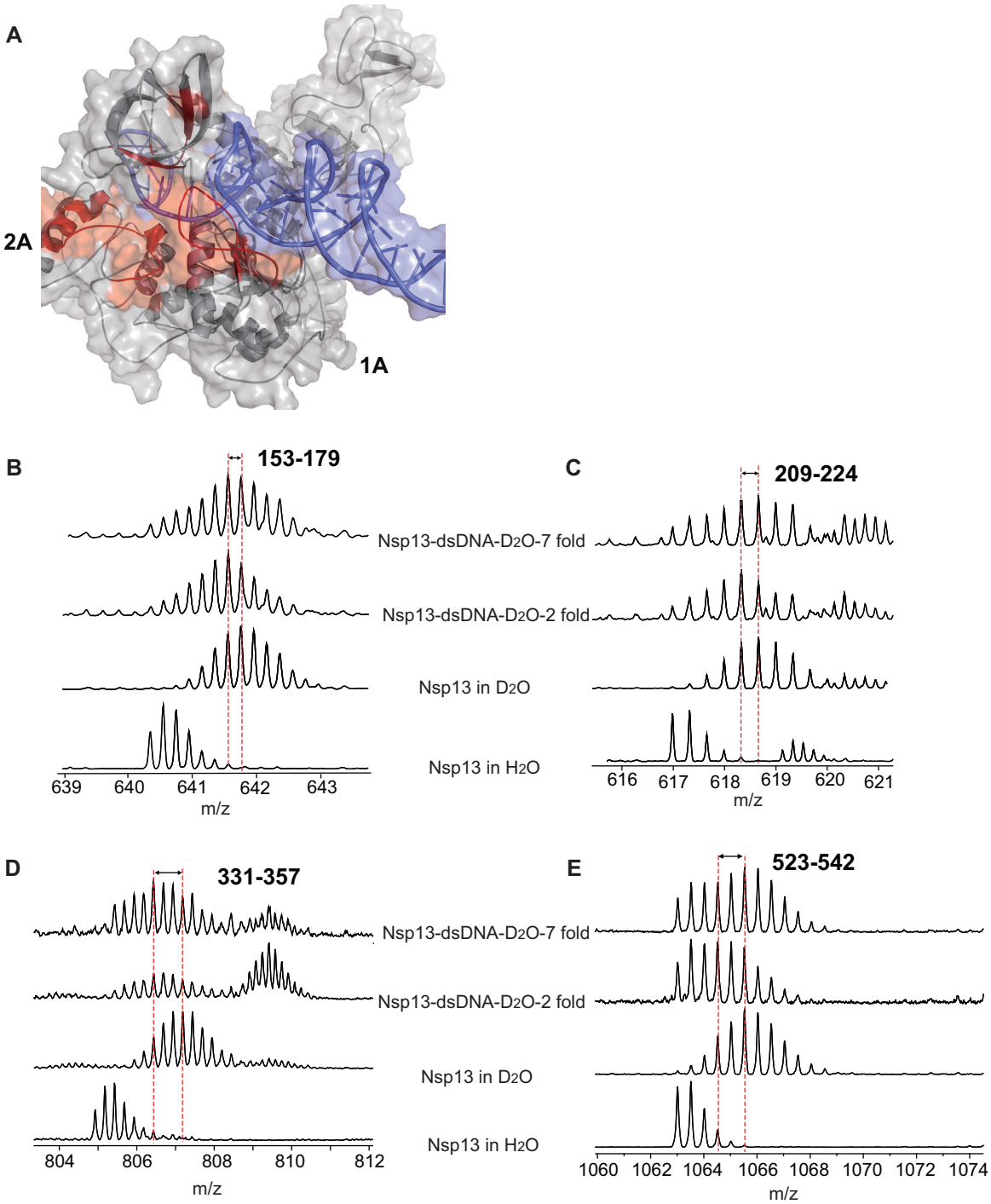

Figure 3. Nucleic acids binding regions. Images B, C, D and E represent results of the H/D exchange experiments recognizing the nucleic acids binding regions. There are four shift patterns for each peptide in different samples where the first and second row represents the shift patterns of SARS-Nsp13 incubated with 7-fold molar and 3-fold molar excess of dsDNA respectively, the third row represents the shift pattern of SARS-Nsp13 and the last row represents the unexchanged pattern of SARS-Nsp13. The x-axes displays the mass-to-charge ratio of each peptide. The dashed vertical lines indicate the mass-to-charge ratio for each peptide in different samples. When the mass-to-charge ratio of SARS-Nsp13 incubated with nucleic acids shifts to right compared to that of SARS-Nsp13, more H/D exchanges in the peptides happen and vice versa. (**A**) Regions in red are the predicted nucleic acids binding related peptides based on the complex model, where the dsDNA is highlighted in blue. (**B**) Shift patterns for peptides 153–179. (**C**) Shift patterns for peptides 209–224. (**D**) Shift patterns for peptides 331–357. (**E**) Shift patterns for peptides 523–542.

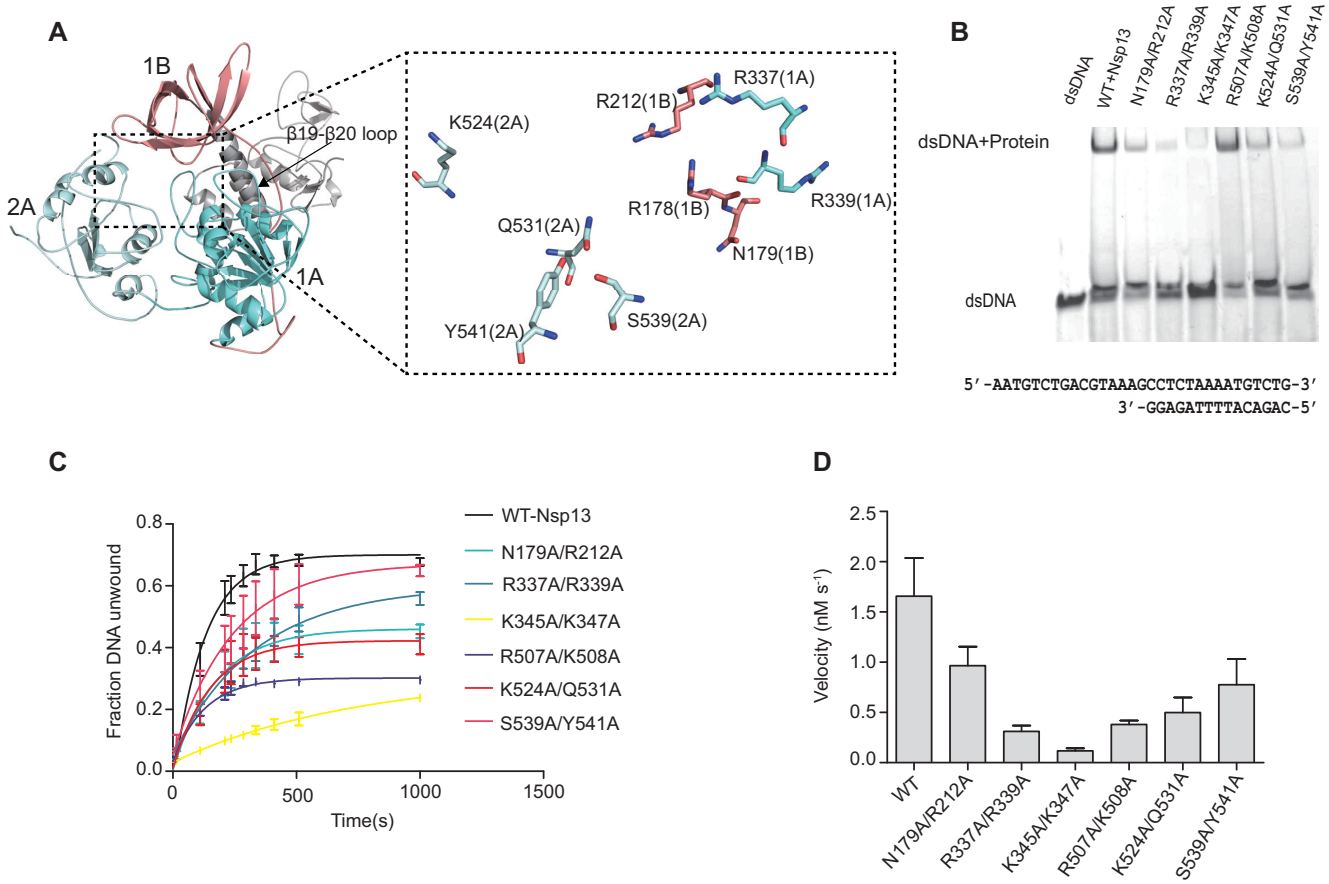

Figure 4. Unwinding activity of double mutants relevant for nucleic acids binding. (**A**) The rectangle indicates the location of amino acid residues involved in nucleic acids binding and the black arrow points to the β19–β20 loop. Residues in salmon belong to the 1B domain. Residues in cyan belong to the 1A domain. Residues in palecyan belong to the 2A domain. All residues are presented in color by elements with S atoms in orange, O atoms in red, N atoms in blue and H atoms in tints. (**B**) The binding affinity to dsDNA of SARS-Nsp13 and six double mutants are demonstrated through EMSA. The protein concentration is 5 μM and the dsDNA concentration is 50 nM. Protein was incubated with dsDNA for 30 min at room temperature. (**C**) The time-course changing of dsDNA unwound fraction for WT-Nsp13 and six double mutants. The initial dsDNA concentration is 400 nM and the protein concentration is 20 nM. The fitting function is one-phase association in the Graphpad Prism program. (**D**) Initial unwinding velocities of WT-Nsp13 and six double mutants under the dsDNA concentration of 400 nM are 1.657 ± 0.6578 nM/s (WT-Nsp13), 0.9663 ± 0.3265 nM/s (N179A/R212A), 0.3105 ± 0.1036 nM/s (R337A/R339A), 0.1184 ± 0.04126 nM/s (K345A/K347A), 0.3797 ± 0.06969 nM/s (R507A/K508A), 0.04992 ± 0.2609 nM/s (K524A/Q531A) and 0.7764 ± 0.4421 nM/s (S539A/Y541A) respectively.

exchanges. The 1A domain is now loosening its grasp on nucleic acid compared to the 2A domain (Figure 5B).

The SARS-Nsp13-dsDNA sample with ADP-AlF_4^- represents a transition state of ATP hydrolysis where AlF_4^- mimicks the gamma-phosphate transition state. The increased H/D exchange in peptides 427–437 (Supplementary Table S1) indicates that the 1A and 2A domains tend to be away from each other. Peptides 318–330 and 358–369 of the 1A domain turn from a relaxed condition in substrate state (blue) to a more tightened condition in transition state (red) when ATP hydrolysis occurs. Taking the two facts into consideration, we can reasonably deduce that the 1A domain slides along the nucleic acid away from 2A domain (Figure 5C).

Next, data was collected for the SARS-Nsp13-dsDNA bound with ADP (product) and it exhibited the largest conformational change since the shift D values in all related regions changed the most. Compared to the transition state, the 1A and 2A domains continued to be away from each other according to the increased H/D exchange in peptides 427–437. The 1A domain reaches its most tightened condition while the two nucleic acid binding related regions on the 2A domain 496–511 and 511–542 showed different H/D exchange patterns where peptides 496–511 exchanged deuterium more and peptides 511–542 exchanged deuterium less. This suggested that the nucleic acid binding region moved towards the 1A domain direction at the end of an ATP hydrolysis cycle (Figure 5D).

The ZBD and stalk domains are critical for the helicase activity of SARS-Nsp13

The 1B, 1A and 2A domains have all been demonstrated to be involved in the dsDNA unwinding process directly or indirectly. Nevertheless, the role of the ZBD and stalk domains remained unclear.

Among the 100 amino acids folding into the ZBD domain, there are 13 cysteines and 3 histidines that play vital roles. The first canonical Zinc Finger(ZnF1) is formed

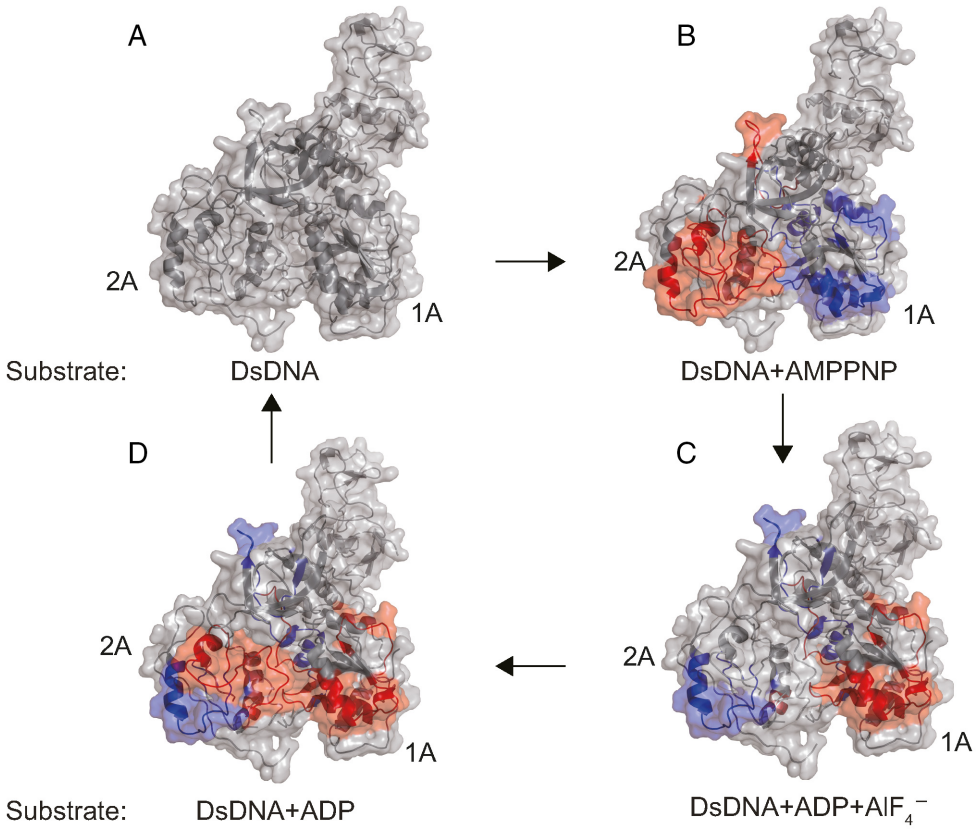

Figure 5. Different states of Nsp13 with different small molecules as indicated by H/D exchange experiment results (Supplementary Table S1). A, B, C and D represent four different conformation states of SARS-Nsp13 with or without small molecules and they form a cycle in which ATP is hydrolysed by step. Regions in red suggest it experienced less H/D exchanges while regions in blue suggest it experienced more compared to the previous state in the cycle. (**A**) The initial state where Nsp13 is bound with dsDNA. (**B**) The substrate state where Nsp13-dsDNA is bound with ATP analog (AMPPNP). (**C**) The transition state where Nsp13-dsDNA is bound with ADP-AlF_4^-. (**D**) The product state where Nsp13-dsDNA is bound with ADP.

by Cys5, Cys8, Cys26 and Cys29. The second Zinc Finger (ZnF2) is made up of Cys16, Cys19, His33 and His39. Lastly, Cys50, Cys55, Cys72 and His75 make up the third Zinc Finger(ZnF3). While ZnF1 and ZnF2 are located at the interface between domain ZBD and 1A, ZnF3 is positioned away and does not interact with other regions of the protein (Figure 6A).

PDB coordinates of the ZBD only was uploaded into the DALI server (25) for structural alignment. According to the result, the ZBD domain of SARS-Nsp13 most resembles the CH domain of Upf1 (hUpf1 PDB code: 2WJY, DALI *Z*-score: 7.9) aside from MERS-Nsp13.

One of the structural characteristics that makes SARS-Nsp13 and Upf1 different is that the CH domain (the counterpart of the ZBD domain) from Upf1 connects with the 1B domain with a rather flexible region consisting of a long α helix and a disordered loop compared to the ZBD domain of SARS-Nsp13, structurally enabling the Upf2 to pull it away from blocking the nucleic acid binding channel (Figure 6B) (12). Yet compared to Upf1, the ZBD domain of SARS-Nsp13 is almost inflexible due to the much shorter loop connecting the ZBD domain and the stalk domain. The way the ZBD domain packs against the stalk domain can also account for its fixed state.

It is obvious that the stalk domain, composed of three tightly interacting α helices (α2, α3, α4) (Supplementary Figure S2), connects the ZBD domain with 1B domain and also forms a small two-sided interface for ZBD domain (α2–α4) and two helicase core domains, mainly 1A domain (α3–α4) with hydrophobic as well as hydrophilic interactions. While lacking flexibility, this spatial arrangement of the stalk domain confers the ZBD domain to regulate the unwinding activity of SARS-Nsp13.

We highlighted all the critical hydrophobic interaction related residues involving the stalk domain. Six of these residues including V6, L7, I20, F106, L130 and A140 cluster together on the α2–α4 interface where the ZBD domain contacts with the stalk domain. How the stalk domain packs against 1A domain can be attributed to all the following residues situated on the α3-α4 interface, 114W, 117A, 120Y, 121I, 130L, 138L, 234P, 235L, 238P, 382Y, 411L, 412L, 417L and 421Y (Figure 6C).

The two residues N102 and K131, involved in hydrophilic interactions between domains, were replaced by alanine in separate experiments, in order to assess their influence on the helicase activity. The interaction between K131 and S424, situated on the α3 helix and 1A domain separately, provides structural stability for the stalk region. N102, signifying the end of the ZBD domain and the beginning of the

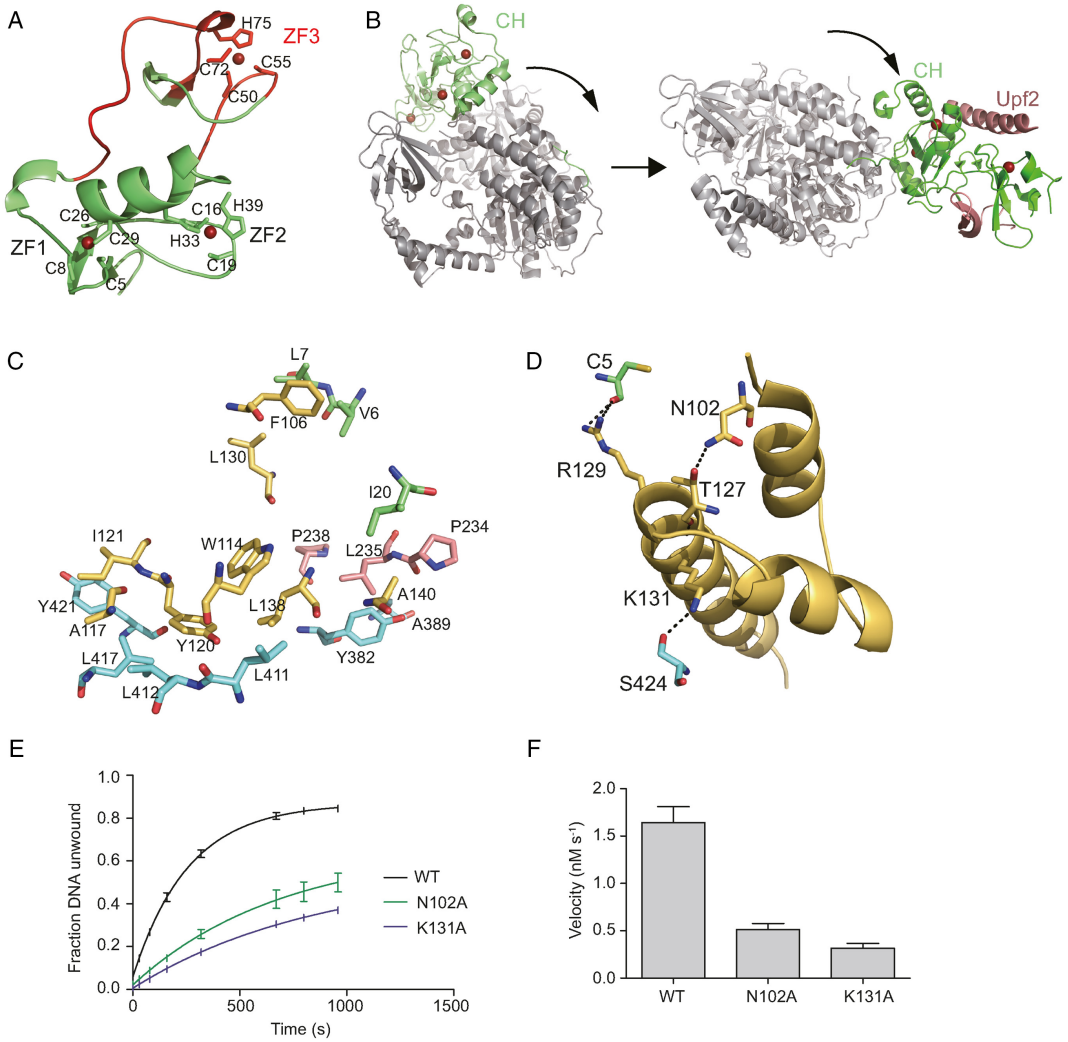

Figure 6. The ZBD domain plays a critical role during the SARS-Nsp13 helicase activity cycle. (**A**) Key residues participating in zinc finger formation. ZF3 motif is highlighted in red. Three zinc atoms are presented in sphere in red. (**B**) How the CH domain of Upf1 is rotated away through interacting with Upf2 (18). The CH domain is highlighted in green. The Upf2 is highlighted in salmon. The left structure represents the Upf1 only while the right structure represents the Upf1–Upf2 complex. (**C**) Hydrophobic residues involved in stalk region packing against ZBD and 1A domains respectively. Residues in green belong to the ZBD domain. Residues in yelloworange belong to the stalk domain. Residues in salmon belong to the 1B domain. Residues in cyan belong to the 1A domain. All residues are presented in color by elements with S atoms in orange, O atoms in red, N atoms in blue and H atoms in tints. (**D**) The two residues N102 and K131 involved in hydrophilic interaction in the stalk domain. Residues in green belong to the ZBD domain. Residues in cyan belong to the 1A domain. The stalk domain is presented in yelloworange. All residues are presented in color by elements with S atoms in orange, O atoms in red, N atoms in blue and H atoms in tints. (**E**) The time-course changing of dsDNA unwound fraction for mutants N102A and K131A. The initial dsDNA concentration is 400 nM and the protein concentration is 20 nM. The fitting function is one-phase association in the Graphpad Prism program. (F) Initial unwinding velocities of WT-Nsp13 and two single mutants under the dsDNA concentration of 400 nM are 1.643 ± 0.1667 nM/s (WT-Nsp13), 0.5119 ± 0.06516 nM/s (N102A) and 0.3164 ± 0.05154 nM/s (K131A) respectively.

stalk domain, interrelates with T127, also a residue of the α3 helix. Both of them showed helicase function deficiency, but to a different degree (Figure 6D).

Based on this analysis it can be concluded that there is a top-to-bottom signal transferring system started by ZBD domain in SARS-Nsp13 which can relay the 'signal' to the helicase core domains.

SARS-Nsp12 can regulate the unwinding process of SARS-Nsp13 through direct interaction

Both being important components of the replication and transcription complex (RTC) of SARS-CoV, there must be functional relationships between SARS-Nsp12 (RdRp) and SARS-Nsp13. We performed the helicase assay of SARS-Nsp13 alone and with SARS-Nsp12, the results of which revealed that SARS-Nsp12 can enhance the unwinding activity of SARS-Nsp13 (Figure 7A and B). The ATPase activity of SARS-Nsp13 alone and with SARS-Nsp12 were also tested and compared (Figure 7C and D). The results demonstrate that MERS-Nsp12 can also enhance the ATPase activity of SARS-Nsp13.

To testify whether SARS-Nsp12 regulates the unwinding process of SARS-Nsp13 directly through interacting with SARS-Nsp13, an SPR assay was conducted. The 0.236 μM

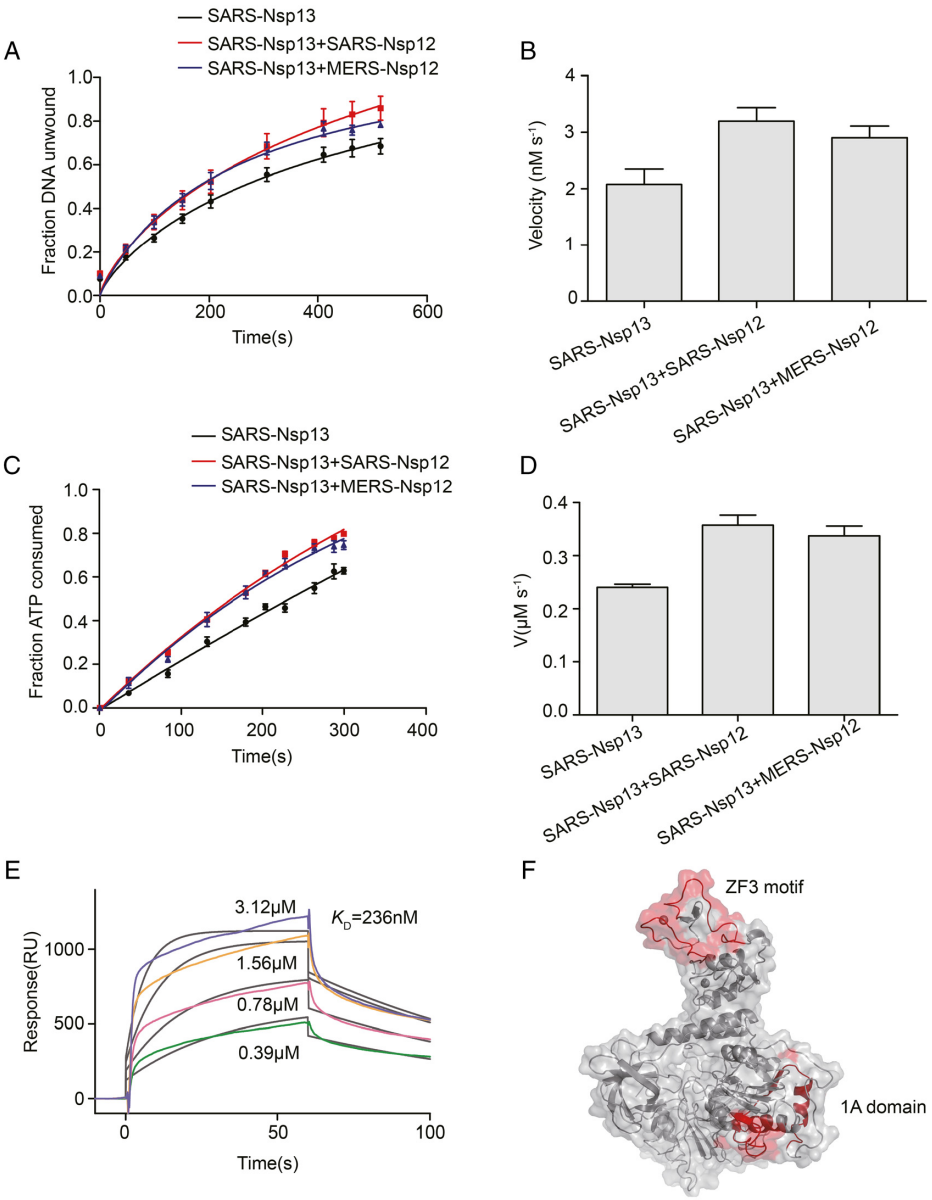

Figure 7. The interaction between SARS-Nsp13 and SARS-Nsp12. (**A**) The unwinding activity of SARS-Nsp13 incubated with SARS-Nsp12 and MERS-Nsp12 is presented as the time-course changing of the dsDNA unwound fraction. The initial dsDNA concentration is 250 nM and the protein concentration is 20 nM. The fitting function is one-phase association in the Graphpad Prism program. (**B**) Initial unwinding velocities of SARS-Nsp13, SARS-Nsp13 with SARS-Nsp12 and SARS-Nsp13 with MERS-Nsp13 under the dsDNA concentration of 400 nM are 2.078 ± 0.4675 nM/s (SARS-Nsp13), 3.199 ± 0.4153 nM/s (SARS-Nsp13 incubated with SARS-Nsp12), 2.905 ± 0.3589 nM/s (SARS-Nsp13 incubated with MERS-Nsp12) respectively. (**C**) ATPase activity of SARS-Nsp13, SARS-Nsp13 with SARS-Nsp12 and SARS-Nsp13 with MERS-Nsp13. The initial ATP concentration is 150 μM and the protein concentration is 25 nM. The changes of percentage of hydrolyzed ATP over time is demonstrated. The fitting function is one-phase association in the GraphPad Prism program. (**D**) ATP hydrolysis velocities of SARS-Nsp13 and SARS-Nsp13 incubated with SARS-Nsp12 or MERS-Nsp12 under 150 μM ATP concentration are 0.2401±0.01062 μM/s (SARS-Nsp13), 0.3572 ± 0.0329 μM/s (SARS-Nsp13 incubated with SARS-Nsp12) and 0.3373 ± 0.0314 μM/s (SARS-Nsp13 incubated with MERS-Nsp12) respectively. (**E**) Representative SPR sensorgrams for SARS-Nsp12 with 3.12 μM SARS-Nsp13 (blue), 1.56 μM SARS-Nsp13 (orange), 0.78 μM SARS-Nsp13 (pink) and 0.39 μM SARS-Nsp13 (green). Association time was 60 s and dissociation time was 60 s. The binding affinity is $K_D = 236$ nM. (**F**) SARS-Nsp12 binding regions on ZF3 motif of ZBD and 1A domains are highlighted in red.

K_d value calculated for SARS-Nsp12 and SARS-Nsp13 without any ligand demonstrated that there exists structural interaction between them, indicating that they function co-operatively *in vivo* (Figure 7C).

Hence, this left us the necessity to identify the binding regions of SARS-Nsp13 to SARS-Nsp12. After comparing H/D exchange patterns of SARS-Nsp13 with SARS-Nsp13 bound to SARS-Nsp12 (Supplementary Figure S7), we identified four peptides to be responsible, peptides 44–56, 71–92, 262–294 and 317–330, located on the ZF3 motif of the ZBD domain and the 1A domain respectively (Figure 7D).

Interestingly, MERS-Nsp12 can also increase the helicase activity of SARS-Nsp13 (Figure 7A and B), suggesting that

the interaction between SARS-Nsp13 and SARS-Nsp12 is conserved across CoVs. We performed the sequence alignment between SARS-Nsp13 and MERS-Nsp13 using ClustalW2 and EsPript3.0 and the conserved residues are highlighted in the alignment result (Supplementary Figure S2) (26,27).

DISCUSSION

Here we have solved the first structure of SARS-Nsp13 and have studied its molecular features that are involved in regulating the unwinding process.

How does the β19–β20 loop participate in the unwinding process?

We characterized the structural and functional information of the NTPase active site on the base between the 1A and 2A domains and the nucleic acid binding channel formed by the 1B, 1A and 2A domains. Amongst the characterized residues for substrate binding, four of them belong to the same β19–β20 loop on the 1A domain. Results of the H/D exchange assay showed that different from binding ssDNA, the β19–β20 loop only changed its shift pattern when incubated with dsDNA. We thus deduced that β19–β20 loop participates in some way in the unwinding process rather than binding. Previous studies showed that virus growth in cells can be attenuated with the introduction of the mutation A335V for MHV-Nsp13 (Mouse Hepatitis Virus-Nsp13) and the viral titer in the liver of infected mice was reduced by 30-fold (28). The counterpart for A335 in MHV is A336 in SARS-Nsp13 according to the alignment and it is also conserved in MERS-Nsp13, HCoV-229E (Human coronavirus 229E) and PHEV (Porcine hemagglutinating encephalomyelitis) (Supplementary Figure S2). The four residues critical for helicase activity R337, R339, K345 and K347 are basic amino acids. Situated on the entrance of nucleic acid binding channel, they can attract negative charged nucleic acid into the channel. The two mutants R337A/R339A and K345A/K347A both provided two additional hydrophobic alanine residues to prevent the entrance of the nucleic acid into the channel. However, A335 provides a proper steric hindrance to destabilize and wedge the double-stranded part of nucleic acid unwound.

The translocation mechanism for SARS-Nsp13 on single-stranded nucleic acid

We can abstract a simple model for the SARS-Nsp13 translocating on single-stranded nucleic acid according to the results of H/D exchange assays of three states namely substrate state, transition state and product state, where only the 1A and 2A domains were involved for conciseness. During the translocation process of SARS-Nsp13, the 1A and 2A domains come close to each other when ATP molecules enters the pocket. The 2A domain tightens the grasp on nucleic acid while the 1A domain loosens the grip on nucleic acid, ready for the next step. At the same time, the 1B domain (166–182) remains grasping the nucleic acid, helping the 1A domain to stabilize the nucleic acid. In the transition state when the hydrolysis occurs, the two domains begin to be taken apart and the more relaxed 1A domain slide along the nucleic acid and regrasps on it when the 1B domain loosen the grip on it. Lastly in the product state, the cleft between the 1A and 2A domains continues to enlarge while one nucleic acid binding region (496–511) on 2A domain loosens and the other region (511–542) tightens. In addition, the 1A domain tightens its grasp on the nucleic acid with the 1B domain also regrasping it.

The translocation model we abstracted for SARS-Nsp13 is consistent with the RecD2 translocation mechanism which is also a member of SF1B (in 5′-3′ direction) yet with low sequence identity with SARS-Nsp13 (29). What is different between the two models is that the 1B domain in SARS-NSP13 functions as a whole with the 1A domain while the 2B domain in RecD2 functions as a whole with its 2A domain. This feature is in accordance with Upf1 since the 1B domain of Upf1 is an inserted domain in the 1A domain.

The ZBD domain is critical for helicase activity or even the life cycle of SARS-CoV

Functional studies showed that Nsp13 from HCoV-229E, belonging to CoVs as SARS-Nsp13, displayed deleterious ATPase activity resulting from Cys or His residues substitutions (C5003A, C5021H, C5024A, H5028R) in the ZBD domain (30). It can be concluded that unlike Upf1, the ZBD domain of nidovirus helicase is indispensable for its catalytic activity and the interplay between ZBD domain and core helicase domains is finely tuned.

In contrast to the flexible CH domain of Upf1, the ZBD domain of SARS-Nsp13 interacts with the stalk domain tightly and plays a vital role in the helicase activity. Structural arrangement of the stalk domain with the 1A and ZBD domains provides strong evidence that the stalk domain can be the rigid bridge transferring the influence coming from the ZBD domain onto the helicase core domains.

The ZBD structural alignment between Upf1 and SARS-Nsp13 showed that they are much alike (*Z* score, 7.9). As an essential component in the NMD pathway in eukaryotic cell, Upf1 is crucial in recognizing exogenous nucleic acid for degradation. SARS-Nsp13 with the much alike ZBD domain might therefore mimic Upf1 to interact with Upf2 to help SARS-CoV to escape the host immune system.

The interaction between SARS-Nsp12 and SARS-Nsp13 is critical for life cycle of CoVs

We have substantiated that all five domains in SARS-Nsp13 are directly or indirectly involved in helicase activity and are finely coordinated with each other due to the well-arranged structural assembly. However, the self-equilibrium of SARS-Nsp13 will be readjusted when it functions *in vivo* since there will be external force imposed on it.

In the life cycle of CoVs, Nsp13 as a helicase would be likely to lead the replication and transcription complex (RTC) to unwind the double-stranded nucleic acid for self-reproduction. There are two facts that provide an opportunity for the first visualization of the RTC of CoVs both functionally and structurally, 1) Both SARS-Nsp12 and MERS-Nsp12 can enhance the helicase and ATPase activity of

SARS-Nsp13; 2) SARS-Nsp12 can interact with SARS-Nsp13 on the ZF3 motif of the ZBD domain and the 1A domain.

DATA AVAILABILITY

Atomic coordinates and structure factors for the reported crystal structures have been deposited with the Protein Data bank under accession number 6JYT.

SUPPLEMENTARY DATA

Supplementary Data are available at NAR Online.

ACKNOWLEDGEMENTS

The authors give their sincere gratefulness to staff at SSRF beamline BL17U and BL19U for their help with crystallographic data collection.

FUNDING

National Major Project Grant [2017YFC0840300]; National Natural Science Foundation of China [81330036, 31570717, 81621005, 81520108019]. Funding for open access charge: National Major Project Grant.
Conflict of interest statement. None declared.

REFERENCES

1. Hilgenfeld,R. and Peiris,M. (2013) From SARS to MERS: 10 years of research on highly pathogenic human coronaviruses. *Antiviral Res.*, **100**, 286–295.
2. Fehr,A.R., Channappanavar,R. and Perlman,S. (2017) Middle east respiratory syndrome: emergence of a pathogenic human coronavirus. *Annu. Rev. Med.*, **68**, 387–399.
3. Marra,M.A., Jones,S.J., Astell,C.R., Holt,R.A., Brooks-Wilson,A., Butterfield,Y.S., Khattra,J., Asano,J.K., Barber,S.A., Chan,S.Y. *et al.* (2003) The Genome sequence of the SARS-associated coronavirus. *Science*, **300**, 1399–1404.
4. Subissi,L., Imbert,I., Ferron,F., Collet,A., Coutard,B., Decroly,E. and Canard,B. (2014) SARS-CoV ORF1b-encoded nonstructural proteins 12–16: replicative enzymes as antiviral targets. *Antiviral Res.*, **101**, 122–130.
5. Shum,K.T. and Tanner,J.A. (2008) Differential inhibitory activities and stabilisation of DNA aptamers against the SARS coronavirus helicase. *Chem. Biol. Chem.*, **9**, 3037–3045.
6. Jang,K.J., Lee,N.R., Yeo,W.S., Jeong,Y.J. and Kim,D.E. (2008) Isolation of inhibitory RNA aptamers against severe acute respiratory syndrome (SARS) coronavirus NTPase/Helicase. *Biochem. Biophys. Res. Commun.*, **366**, 738–744.
7. Adedeji,A.O., Singh,K., Kassim,A., Coleman,C.M., Elliott,R., Weiss,S.R., Frieman,M.B. and Sarafianos,S.G. (2014) Evaluation of SSYA10-001 as a replication inhibitor of severe acute respiratory syndrome, mouse hepatitis, and middle east respiratory syndrome coronaviruses. *Antimicrob. Agents Ch.*, **58**, 4894–4898.
8. Fairman-Williams,M.E., Guenther,U.P. and Jankowsky,E. (2010) SF1 and SF2 helicases: family matters. *Curr. Opin. Struct. Biol.*, **20**, 313–324.
9. Ivanov,K.A., Thiel,V., Dobbe,J.C., van der Meer,Y., Snijder,E.J. and Ziebuhr,J. (2004) Multiple enzymatic activities associated with Severe acute respiratory syndrome coronavirus helicase. *J. Virol.*, **78**, 5619–5632.
10. Tanner,J.A., Watt,R.M., Chai,Y.B., Lu,L.Y., Lin,M.C., Peiris,J.S., Poon,L.L., Kung,H.F. and Huang,J.D. (2003) The severe acute respiratory syndrome (SARS) coronavirus NTPase/helicase belongs to a distinct class of 5′ to 3′ viral helicases. *J. Biol. Chem.*, **278**, 39578–39582.
11. Adedeji,A.O., Marchand,B., Te Velthuis,A.J., Snijder,E.J., Weiss,S., Singh,K. and Sarafianos,S.G. (2012) Mechanism of nucleic acid unwinding by SARS-CoV helicase. *PLoS One*, **7**, e36521.
12. Clerici,M., Mourao,A., Gutsche,I., Gehring,N.H., Hentze,M.W., Kulozik,A., Kadlec,J., Sattler,M. and Cusack,S. (2009) Unusual bipartite mode of interaction between the nonsense-mediated decay factors, UPF1 and UPF2, *EMBO J.*, **28**, 2293–2306.
13. Deng,Z.Q., Lehmann,K.C., Li,X.R., Feng,C., Wang,G.Q., Zhang,Q., Qi,X.X., Yu,L., Zhang,X.L., Feng,W.H. *et al.* (2014) Structural basis for the regulatory function of a complex zinc-binding domain in a replicative arterivirus helicase resembling a nonsense-mediated mRNA decay helicase. *Nucleic Acids Res.*, **42**, 3464–3477.
14. Hao,W., Wojdyla,J.A., Zhao,R., Han,R.Y., Das,R., Zlatev,I., Manoharan,M., Wang,M.T. and Cui,S. (2017) Crystal structure of Middle East respiratory syndrome coronavirus helicase. *PLoS Pathog.*, **13**, e1006474.
15. Singleton,M.R., Dillingham,M.S. and Wigley,D.B. (2007) Structure and mechanism of helicases and nucleic acid translocases. *Annu. Rev. Biochem.*, **76**, 23–50.
16. Kabsch,W. (1993) Automatic processing of rotation diffraction data from crystals of initially unknown symmetry and cell constants. *J. Appl. Crystallogr.*, **26**, 795–800.
17. Schneider,T.R. and Sheldrick,G.M. (2002) Substructure solution with SHELXD. *Acta Crystallogr. D*, **58**, 1772–1779.
18. Adams,P.D., Grosse-Kunstleve,R.W., Hung,L.W., Ioerger,T.R., McCoy,A.J., Moriarty,N.W., Read,R.J., Sacchettini,J.C., Sauter,N.K. and Terwilliger,T.C. (2002) PHENIX: building new software for automated crystallographic structure determination. *Acta Crystallogr. D. Biol. Crystallogr*, **58**, 1948–1954.
19. Emsley,P. and Cowtan,K. (2004) Coot: model-building tools for molecular graphics. *Acta Crystallogr. D. Biol. Crystallogr*, **60**, 2126–2132.
20. Chalmers,M.J., Busby,S.A., Pascal,B.D., He,Y.J., Hendrickson,C.L., Marshall,A.G. and Griffin,P.R. (2006) Probing protein ligand interactions by automated hydrogen/deuterium exchange mass spectrometry. *Anal. Chem.*, **78**, 1005–1014.
21. Hebling,C.M., Morgan,C.R., Stafford,D.W., Jorgenson,J.W., Rand,K.D. and Engen,J.R. (2010) Conformational analysis of membrane proteins in phospholipid bilayer nanodiscs by hydrogen exchange mass spectrometry. *Anal. Chem.*, **82**, 5415–5419.
22. Tuszynska,I., Magnus,M., Jonak,K., Dawson,W. and Bujnicki,J.M. (2015) NPDock: a web server for protein-nucleic acid docking. *Nucleic Acids Res.*, **43**, W425–W430.
23. Macke,T.J. and Case,D.A. (1998) Modeling unusual nucleic acid structures. *ACS Sym. Ser.*, **682**, 379–393.
24. Chakrabarti,S., Jayachandran,U., Bonneau,F., Fiorini,F., Basquin,C., Domcke,S., Le Hir,H. and Conti,E. (2011) Molecular mechanisms for the RNA-Dependent ATPase activity of Upf1 and its regulation by Upf2. *Mol. Cell*, **41**, 693–703.
25. Holm,L. and Laakso,L.M. (2016) Dali server update. *Nucleic Acids Res.*, **44**, W351–W355.
26. Chojnacki,S., Cowley,A., Lee,J., Foix,A. and Lopez,R. (2017) Programmatic access to bioinformatics tools from EMBL-EBI update: 2017. *Nucleic Acids Res.*, **45**, W550–W553.
27. Gouet,P., Courcelle,E., Stuart,D.I. and Metoz,F. (1999) ESPript: analysis of multiple sequence alignments in PostScript. *Bioinformatics*, **15**, 305–308.
28. Zhang,R., Li,Y.Z., Cowley,T.J., Steinbrenner,A.D., Phillips,J.M., Yount,B.L., Baric,R.S. and Weiss,S.R. (2015) The nsp1, nsp13, and M proteins contribute to the hepatotropism of murine coronavirus JHM.WU. *J. Virol.*, **89**, 3598–3609.
29. Saikrishnan,K., Powell,B., Cook,N.J., Webb,M.R. and Wigley,D.B. (2009) Mechanistic basis of 5′-3′ translocation in SF1B helicases. *Cell*, **137**, 849–859.
30. Seybert,A., Posthuma,C.C., van Dinten,L.C., Snijder,E.J., Gorbalenya,A.E. and Ziebuhr,J. (2005) A complex zinc finger controls the enzymatic activities of nidovirus helicases. *J. Virol.*, **79**, 696–704.